

Near-Infrared Photometry of four stellar clusters in the Small Magellanic Cloud ¹

Alessio Mucciarelli

Dipartimento di Astronomia, Università degli Studi di Bologna, Via Ranzani, 1 - 40127 Bologna, ITALY

`alessio.mucciarelli@studio.unibo.it`

Livia Origlia

INAF - Osservatorio Astronomico di Bologna, Via Ranzani, 1 - 40127 Bologna, ITALY

`livia.origlia@oabo.inaf.it`

Claudia Maraston

Institute of Cosmology and Gravitation, University of Portsmouth, Mercantile House, Hampshire Terrace, P01 2EG, Portsmouth, United Kingdom

`claudia.maraston@port.ac.uk`

Francesco R. Ferraro

Dipartimento di Astronomia, Università degli Studi di Bologna, Via Ranzani, 1 - 40127 Bologna, ITALY

`francesco.ferraro3@unibo.it`

ABSTRACT

We present high-quality J, H and K_s photometry of four Small Magellanic Cloud stellar clusters with intermediate ages in the 1–7 Gyr range (namely NGC 339, 361, 416 and 419) . We obtained deep Color-Magnitude Diagrams to study the evolved sequences and providing a detailed census of the Red Giant Branch (RGB), Asymptotic Giant Branch (AGB) and Carbon star populations in each cluster and their contribution to the total cluster light. We find that in the ~ 5 –7 Gyr old clusters AGB stars account for $\sim 6\%$ of the total light in K_s -band, Carbon stars are lacking and RGB stars account for $\sim 45\%$ of the total bolometric luminosity. These empirical findings are in good agreement with the theoretical predictions. Finally, we derived photometric metallicities computed by using the properties of the RGB and finding an iron content of $[\text{Fe}/\text{H}] = -1.18, -1.08, -0.99$ and -0.96 dex for NGC 339, 361, 416 and 419 respectively.

Subject headings: Magellanic Clouds — globular clusters — techniques: photometry

1. Introduction

The history and the evolution of the Large and Small Magellanic Clouds (LMC and SMC, respectively) are intimately related to the gravitational interactions between the two Clouds and the Milky Way. In particular, the main episodes of star formation enhancement in the SMC are triggered by the near, perigalactic passages of the LMC and of the Milky Way (Harris & Zaritsky 2004; Zaritsky & Harris 2004). The epoch and rate of the main star formation episodes in the Magellanic Clouds (MCs) are still matter of debate and several scenarios have been proposed. For the SMC, while Harris & Zaritsky (2004) suggest 3 episodes occurred 400 Myr, 3 Gyr and 9 Gyr ago, Dolphin et al. (2001) favor a more continuous star formation in the halo with a dominant episode 5–8 Gyr ago. Rafelski & Zaritsky (2005) argue that the cluster age distribution shows a few peaks, but no significant *gaps* as in the LMC (see also Chiosi et al. 2006).

MCs host a globular cluster system which includes objects with different age and metallicity, thus representing a formidable probe of the various stellar populations in the MCs as well as ideal templates for the study of stellar evolution and population synthesis. In this respect, the near-infrared (IR) spectral range is particularly suitable to sample the evolved stellar sequences, whose giant stars are characterized by low surface gravities and effective temperatures.

In our previous papers (Ferraro et al. 2004; Mucciarelli et al. 2006, hereafter Paper I and Paper II, respectively) the near-IR Color-Magnitude Diagrams (CMDs) of 19 young-intermediate age LMC clusters (from ~ 80 Myr to ~ 3 Gyr) have been analysed, providing a quantitative estimate of the AGB and RGB contributions to the total light, as a function of the cluster age. The AGB contribution to the total luminosity starts to be significant at ~ 200 Myr, with a maximum ($\sim 80\%$) at ~ 500 - 600 Gyr. At this same epoch the RGB phase transition occurs and for ages older than 1 Gyr the RGB itself becomes fully developed, while the contribution of AGB is progressively reduced.

The present paper reports the results for four SMC clusters belonging to the intermediate-age population of the SMC. The principal aims of this work are the study of the main features of their near IR CMDs and the contribution to the total cluster luminosity of the AGB and

¹Based on observations collected at La Silla ESO Observatory under proposal 076.D-0381(B).

RGB stars. This sample of SMC clusters allows to check the contribution of the AGB and RGB stars for clusters in an age range (~ 5 -7 Gyr) not covered by the LMC cluster system (because it corresponds to the so-called *Age-Gap*), thus providing complementary information.

The paper is organized as follows: Sect. 2 describes the observations and photometric analysis. Sect. 3 presents the near-IR CMDs and their main features, the inferred metallicities and the integrated magnitudes. Sect. 5 describes the procedure adopted to estimate the completeness correction and the field decontamination. Sect. 6 describes the detailed census of the AGB and Carbon stars in each cluster, and their contribution to the total luminosity, while Sect. 7 analyzes the RGB stellar population.

2. Observations and data reduction

A set of J, H and K_s images of four stellar clusters (namely NGC 339, 361, 416 and 419) in the SMC has been selected at the European Southern Observatory (ESO), La Silla, on 2006 January 1-3 (Program ID: 076.D-0381(B)), by using the NTT 3.5m telescope and the near IR imager/spectrometer SOFI, equipped with a 1kx1k HAWAII array detector. All the observations have been performed by using 0.292''/pixel scale, providing a $\sim 5'' \times 5''$ field of view each frame.

Total integration times of 4min in J, 8min in H and 16min in K_s (split into sets of shorter exposures) have been secured, allowing to reach a magnitude threshold of J ~ 19 and H and $K_s \sim 18.5$. All the secured images have been roughly centered on the cluster center. Moreover, for each target cluster, a control field (a few arcminutes away from each cluster center) has been observed adopting the same instrumental configuration; these field images have been used to construct median-average sky frames. High signal-to-noise flat fields in each band have been acquired by using a halogen lamp alternatively swichted on and off. The final cluster and field frames have been sky-subtracted and flat-field corrected. The observations have been obtained in good seeing conditions (0.6''-0.7'' on average)². The point spread function fitting procedure has been performed by using the ALLSTAR routine of the DAOPHOT (Stetson 1987) reduction package. The detection of the stellar sources has been performed in the J image, then this list of stellar objects has been used as reference for the reduction of the images in the other two filters. The output catalog, obtained by cross-correlating the single-filter catalogs, includes all stars measured in at least two

²Only for the cluster NGC 361 the observations have been performed in worse seeing conditions ($\sim 1''$) limiting the magnitude threshold to $K_s \sim 18$.

bands. The instrumental magnitudes have been transformed into the Two-Micron All-Sky Survey (2MASS) photometric system, by using the large number of stars (a few hundreds) in common between SOFI and the 2MASS. No significant color term in each band has been found. Finally, the brightest stars that turned out to be saturated in the SOFI images have been recovered from the 2MASS catalog (the typical saturation limit in our images is $K_s \sim 11$). A final catalog listing ~ 1500 - 2500 stars has been obtained in each program cluster. Each cluster center of gravity C_{grav} (see Table 1) has been computed by averaging the α - and δ -coordinates of stars lying within a fixed radius (typically $\sim 90''$) from a guess center (estimated by eye).

3. The CMDs

Fig. 1 reports the $(K_s, (J-K_s))$ CMDs of the four clusters of our sample. For each cluster the age s-parameter ³ (Elson & Fall 1985) is also reported; Fig. 2 shows the CMDs of the corresponding control fields. For each cluster, Table 1 summarizes the coordinates of the center of gravity and other cluster properties, in particular:

(i) *reddening*: for 3 stellar clusters (namely NGC 416, 339 and 361) we adopted the $E(B-V)$ computed by Mighell, Sarajedini & French (1998), from optical WFPC2@HST CMDs. For NGC 419 the typical reddening value of the SMC (Hunter et al. 2003) has been adopted. However, it is worth noticing that the small amount of reddening in the direction of these clusters has a negligible impact on the near IR photometry.

(ii) *age*: as already discussed in Paper I and II, the lack of a homogeneous age scale for the Magellanic clusters based on the measurement of the Main Sequence Turn-Off represents a severe limitation. Accordingly to Paper I and II, we adopted the Elson & Fall (1985) s-parameters as an age indicator and the most recent age calibration derived by Girardi et al. (1995): $\log(\text{Age}) = 6.227 + 0.0733 \cdot s$. By using WFPC2@HST photometry, Mighell, Sarajedini & French (1998) derived Turn-Off ages for NGC 339, 361 and 416 in the 5–7 (± 1.1 – 1.3) Gyr range (see Table 1). Recently, new determinations of the ages of NGC 339, 416 and 419 have been presented by Glatt et al. (2008), based on high-resolution ACS@HST photometry, deriving an age of 6 Gyr for the first 2 clusters. In the case of NGC 419 the authors list only an age range (between 1.2 and 1.6 Gyr) because of the complex Turn-Off morphology. This age is also in agreement with the previous estimate (see Rich et al. 2000). All the direct age estimates are consistent with those inferred from the s-parameter.

³The so-called s-parameter, defined by Elson & Fall (1985) represents an extension of the SWB classification, introduced by Searle, Wilkinson, & Bagnuolo (1980) to date the Magellanic clusters and based on the position of the clusters in the $(U-B)_0$ - $(B-V)_0$ plane.

The main features of these CMDs are summarized as follows:

- (1) an extended and fully populated RGB;
- (2) a bulk of stars at $K_s \sim 17.5$, corresponding to the He-Clump;
- (3) the brightest objects with $K_s < 13$ are likely AGB stars;
- (4) the cluster and field population have similar features.

The presence of a well-defined and populated RGB in each cluster is in agreement with the relatively old age of the clusters which have already experienced the RGB phase transition (as discussed in Paper I and II). We note that the CMDs of NGC 416 and of its surrounding field show a blue stellar population (located at $(J-K_s) \sim -0.1$ and with stars brighter than $K_s \sim 16.5$). This younger population has been also detected in the optical photometry presented by Mighell, Sarajedini & French (1998).

4. Metallicity

As well known the properties (morphology and position) of the RGB are sensitive function of the overall metallicity of the population. Hence, the presence of a well populated RGB in the CMDs shown in Fig. 1 allows us to derive a photometric measure of the cluster metallicity. Recently, Valenti, Ferraro & Origlia (2004) have presented a calibration of a set of morphological RGB parameters (in the IR plane) in terms of the cluster metallicity for a sample of old Galactic globular clusters, by adopting both the Carretta & Gratton (1997) iron metallicity scale and the global metallicity $[M/H]$, as computed by taking into account the enhancement of the α -elements. Since the few available chemical information for the SMC stellar population indicate solar scaled value of the $[\alpha/Fe]$ abundance ratio (see Hill 1997), we use the $[Fe/H]$ scale as reference. We used the entire set of RGB parameters defined by Valenti, Ferraro & Origlia (2004) in the IR planes (K_s , $J-K_s$) and (H, $J-H$), namely the $(J - K_s)_0$ color at different absolute magnitudes $M_K = (-3, -4, -5, -5.5)$, the $(J - H)_0$ color at $M_H = (-3, -4, -5, -5.5)$, the K_s absolute magnitude at fixed $((J - K_s)_0) = 3$, the H absolute magnitude at $(J - H)_0 = 3$ and the slope of the RGB. All the photometric parameters have been measured along the RGB cluster mean ridge lines. These fiducial ridge lines have been computed following the procedure described in Ferraro et al. (1999); Valenti, Ferraro & Origlia (2004). First, we selected (by eye) stars belonging to the RGB in order to exclude He-clump, AGB and field stars, then the second-order polynomial has been fitted to the observed distribution. The ridge line has been transformed into the absolute plane by adopting a distance modulus of $(m - M)_0 = 18.99$ (Cioni et al. 2000), the reddening listed in Table 1 and the extinction law by Rieke & Lebofsky (1985). Once the photometric

parameters were measured, the various estimates of the cluster metallicity were computed from the equations listed in Appendix A of Valenti, Ferraro & Origlia (2004). All these estimates turn out to be consistent one to each other (with average dispersion of ~ 0.1), so we assumed for each cluster metallicity the mean value (and reported in Table 2), thus finding $[\text{Fe}/\text{H}] = -1.18, -1.08, -0.99$ and -0.96 dex for NGC 339, 361, 416 and 419, respectively.

Mighell, Sarajedini & French (1998) give a photometric estimate of the cluster metallicity by using the RGB slope in the optical plane (see Table 1). We find their metallicities to be ~ 0.3 dex more metal-poor than ours; this discrepancy can be mainly ascribed to the different adopted metallicity scales. Indeed, the relations by Valenti, Ferraro & Origlia (2004) are calibrated on the Carretta & Gratton (1997) scale, while the $\text{slope}_{\text{RGB}} - [\text{Fe}/\text{H}]$ relation by Mighell, Sarajedini & French (1998) is on the Zinn & West (1984) scale.

4.1. Integrated Magnitudes

In order to compute the integrated magnitudes of the target clusters, we performed aperture photometry, with different aperture radii centered on the center of gravity. A crucial step in this procedure is the correct decontamination from the field population. To do this we performed an equivalent aperture photometry on each control field. The resulting field luminosity has been subtracted to the cluster luminosity. The instrumental integrated magnitude was then calibrated into the 2MASS system following the procedure described in Sect. 2.

For each cluster, Table 2 lists the integrated K_s magnitude, $(J - K_s)$ and $(H - K_s)$ colors and the K_s and bolometric luminosities, as computed by adopting an aperture radius representative of the entire cluster extension (typically 90-100")⁴.

The formal error in the integrated magnitudes can be obtained as the quadrature sum of the photometric error associated to the task PHOT and the uncertainty in the aperture centering. The latter has been estimated by computing aperture photometry using 4 different centers, shifted by ± 5 pixels with respect to the C_{grav} coordinates. Typically, we estimated an error of $\sigma \sim 0.04$ - 0.05 mag in each band, that translates in a errorbar of ~ 0.07 mag in color.

Total luminosities (in K_s -band and bolometric) have been computed by using the integrated magnitudes and adopting a distance modulus for the SMC of $(m - M)_0 = 18.99$ (Cioni et al. 2000), bolometric corrections (by using the $(J - K_s)_0$ color) empirically cal-

⁴In all the clusters the bulk of the luminosity lies within a ~ 50 - $60''$ radius

ibrated by Montegriffo et al. (1998) and solar values of $M_{\odot}^{Bol} = 4.75$ and $M_{\odot}^K = 3.41$. In the following all the derived luminosities are expressed in units of $10^4 L_{\odot}$. The main sources of error in this case are the uncertainty in the integrated magnitudes and in the bolometric corrections (an additional variation of $\sim 10\%$) which translate into a $\sim 5\%$ and $\sim 10\%$ uncertainty in luminosity.

5. Star counts and population ratios

In order to estimate the RGB and AGB contributions to the total cluster light, we use star counts and population ratios, as obtained by adopting suitable *selection boxes* for each evolutionary sequence (He-Clump, RGB and AGB), as discussed in Sect. 6 and 7 (see also Paper I and II). Two main effects must be taken into account in the definition of these quantities, the incompleteness of the photometric catalog and the contamination by field stars.

5.1. Completeness and field decontamination

The degree of completeness can be quantified by adopting the widely-used artificial star technique, discussed in Mateo (1988). For each cluster we have derived the RGB fiducial line and then a population of artificial stars, having magnitudes, colors, and luminosity functions resembling the observed distributions has been generated and added to the original images (by using the DAOPHOT task ADDSTAR). The frame area sampling the cluster has been divided in 3 concentric regions with radii $r < 20''$, $20'' \leq r < 60''$ and $60'' \leq r < 90''$, in order to take into account different crowding conditions and the completeness has been estimated independently in each of them. The maximum spatial extension of each cluster has been estimated from the cluster radial density profile. A total of $\sim 200,000$ artificial stars have been simulated in each cluster in about 1000 simulation runs. Indeed, in order to not alter the crowding conditions, ~ 100 -200 stars have been simulated in each run, corresponding to $\sim 10\%$ of the total stellar population. The fraction of recovered objects in each magnitude interval has been estimated as $\Lambda = \frac{N_{rec}}{N_{sim}}$: the completeness curve was obtained in each radial subregion and shown in Fig. 3. The correction for incompleteness in each radial region was performed by dividing each observed distribution by the corresponding Λ factor. The total number of stars has been obtained by summing the number of stars in each subregion.

It is worth noticing that this procedure allows to take into account only the loss of faint stars due to the crowding but not the possible excess of bright stars due to blending effects

of two or more faint stars into a brighter one. However, this latter effect is marginal in the near IR.

Another important effect which needs to be investigated, is the degree of contamination of the selected samples by the foreground/background stars. In this paper we have applied a statistical decontamination, by using a control field adjacent to the cluster. The total number of stars observed in each evolutionary sequence (AGB, RGB and He-clump) has been counted accordingly to the *selection boxes* both in the cluster and field CMDs, and corrected for incompleteness (see above). The star counts in the field population have been scaled to take into account the different surveyed area, and their contribution have been subtracted from the cluster population.

In summary, for each radial region, each selection box corresponding to each evolutionary stage has been divided in bins of magnitude (typically 0.2 mag wide). Then, the "corrected" number of stars in each bin has been computed as follows:

$$n_{corr} = n_{obs} + (n_{obs}(1/\Lambda - 1)) - n_f$$

where n_{obs} is the number of stars observed in that bin, the second term is the number of stars lost for incompleteness, n_f is the expected number of field stars. The total luminosity of each evolutionary stage can be computed accordingly to the following relation:

$$L_{corr} = \left(\sum_{i=1}^n L_i^{obs} \right) + (n_{comp} \times L_{eq}) - (n_f \times L_{eq})$$

where the term $\sum_{i=1}^n L_i^{obs}$ is the total luminosity of stars observed in a given bin, n_{comp} is the number of stars lost for incompleteness, n_f is the expected number of field stars, and L_{eq} is the equivalent luminosity of that bin, that is the luminosity of a star with magnitude equal to the mean value of the bin.

Finally, star counts and total luminosity of each evolutionary stage have been obtained by summing the contribution of all the bins.⁵

6. The AGB and C-stars population

The AGB stars are the main contributors to the integrated SSP light between $\sim 10^8$ and $\sim 10^9$ yrs (Renzini & Buzzoni 1986; Maraston 1998). AGB stars are initially Oxygen-rich,

⁵The typical errors for the different population ratios (by number and luminosities) have been estimated accordingly to the following formula $\sigma_R = \frac{\sqrt{R^2 \cdot \sigma_D^2 + \sigma_N^2}}{D}$ with $R = N/D$, N being the numerator and D the denominator of the ratio, and by assuming that star counts follow a Poisson statistics.

but if massive enough (with an initial mass $M > \sim 2M_{\odot}$) a star undergoes the so-called *Third Dredge-Up* event during the Thermal-Pulse (TP-AGB) phase, and freshly processed Carbon is carried to the surface, producing a C-rich AGB star.

Frogel et al. (1990) analyzed 39 Magellanic clusters in order to identify AGB stars and concluded that up to 40% of the bolometric luminosity comes from stars with $M_{bol} < -3.6$, likely belonging to the TP-AGB phase. In Paper II we studied the AGB population in the young-intermediate LMC clusters (with ages less than ~ 3 Gyr), finding that the maximum contribution of the AGB to the cluster light occurs at an age of ~ 500 -700 Myr, with a dominant contribution from the C-stars population.

We classify AGB stars only those stars that satisfy the 3 following *criteria*:

- (1) stars brighter than $(K_s)_0 = 12.62$ (corresponding to the RGB tip level for the SMC, see Cioni et al. 2000), in order to minimize the impact of possible RGB stars contamination;
- (2) in order to separate the cluster stars and the most bright background/foreground stars, only stars located in the box showed in Fig. 4 are considered;
- (3) stars located within the cluster extension (see Sec. 4.1).

In order to accurately select C-stars in each cluster, we adopted as a diagnostic tool the $(J-H)_0$ - $(H-K_s)_0$ color-color diagram. Left panel of Fig. 4 shows the cumulative $(J-H)_0$ - $(H-K_s)_0$ diagram for all the selected AGB stars, with overplotted the box defined from Bessell & Brett (1988) to isolate the mean locus of the C stars and long period variables (LPV), and the mean locus for the K giant stars defined by Frogel et al. (1978). All the stars flagged as C-stars show very red $(J-K_s)$ colors also in the 2MASS database, thus excluding major errors in the PSF-fitting procedure. The adopted methodology to identify and distinguish C and O-stars is also consistent with the criterion adopted by Cioni & Habing (2003), who based their selection on the $J-K_s$ color only and targeting C-stars does brighter than the RGB-Tip and with $(J-K_s) > 1.3$.

Right panel of Fig. 4 shows the cumulative CMD for the four clusters of the sample with overplotted the box used for the selection: the candidate AGB stars are marked (grey points for the O-rich and black points for the C-rich stars). In the following we summarize the census of the AGB stars in each cluster:

- *NGC 416*— Only 1 AGB (O-rich) star has been identified in this cluster. The other bright stars detected in the field of view are located too far away from the cluster center (at $> 100''$), hence they are unlikely cluster members.
- *NGC 419*— This cluster exhibits a large population of candidate AGB stars, already studied by Frogel et al. (1990) who identified 10 C-stars likely members. We found

21 AGB stars, 12 C-stars, 4 likely LPVs, within $\sim 90''$ from the cluster center. None of the LMC clusters previously studied (Paper II) shows a comparable number of C-stars. The paucity of C-stars in the observed LMC clusters with the same age could be ascribed to a metallicity effect (see Fig. 5 in Maraston 2005). We note that outside the cluster radius only 3 O-rich AGB stars have been detected and none C-stars.

- *NGC 339*— One O-rich AGB star has been detected, just above the RGB Tip.
- *NGC 361*— Only one AGB (O-rich) star has been identified.

A possible source of error in the computation of the AGB counts and luminosities is the location of the RGB Tip: however, a variation of 0.2 mag implies the inclusion of a few fainter AGB stars only (with a variation in the total AGB luminosity $< 10\%$).

Table 3 lists the final star counts and luminosities of the AGB and C stars in each cluster. Fig. 5 (top panel) shows the K_s -band luminosity of the AGB stars normalized to the total luminosity as a function of age (black points); for comparison the values obtained for the LMC clusters in Paper II are also plotted (grey points). It is worth noticing the higher ($\sim 50\%$) luminosity ratio of NGC 419 compared to the value ($\sim 10\%$) of the other 3, significantly older clusters. Fig. 5 (bottom panel) shows the same distribution but binned in age as discussed in Paper II for what concerns the LMC clusters, while only three out of four SMC clusters, in our sample namely NGC 339, 361 and 416, with similar ages have been binned.

Theoretical predictions computed by Maraston (1998, 2005) for $[M/H] = -0.33$ (solid line) and -1.35 dex (dashed line) are also plotted for comparison. The theoretical AGB and RGB population ratios have been computed by using SSP models by Maraston (1998) and Maraston (2005), obtained with an evolutionary code that estimates the energetics of any post-main-sequence stage by following the prescriptions of the *fuel consumption theorem* defined by Renzini & Buzzoni (1986) (see also Ferraro et al. (2004) for more details).

Similarly, Fig. 6 shows the K_s -band luminosity of the C-stars only, normalized to the total luminosity, as a function of age. Note that in NGC 419 $\sim 80\%$ of the AGB light is provided by the C-stars population.

We thus confirm previous results discussed by Frogel et al. (1990) that C-stars are only detectable in relatively young (< 2 Gyr) clusters of IV-VI SWB Type and theoretical predictions which require a minimum envelope mass for the occurrence of the *Third Dredge-Up*. Stars with $< 1.2 M_\odot$ initial mass have a residual (if any) envelope mass which is too small to experience the *Third Dredge-Up*.

7. The RGB population

In order to calculate the RGB population ratios we adopted the same procedure used in Paper I and II. Three observables have been identified to study the degree of development of the RGB as a function of age and metallicity: (i) the number of RGB stars normalized to the number of He-Clump stars (N_{RGB}/N_{He-Cl}), (ii) the bolometric luminosity of the RGB normalized to the He-Clump one ($L_{RGB}^{bol}/L_{He-Cl}^{bol}$), and (iii) the bolometric luminosity of the RGB normalized to the total cluster luminosity ($L_{RGB}^{bol}/L_{TOT}^{bol}$). In order to identify the mean loci of the upper RGB and He-Clump stars, we use the cumulative, dereddened $K_0-(J-K)_0$ CMD as a diagnostic diagram. As in Paper I and II (see their Fig. 5 and Fig. 9 respectively) we define two boxes for these evolutionary stages. The size of each box has been defined to sample the bulk of the population, assuming to be ~ 5 times the photometric uncertainty at a given level of magnitude. The upper limit of the RGB box is the magnitude of the RGB Tip, the same used to define the bottom limit of the AGB box (Sect. 6).

The final population ratios (by counts and luminosities) have been computed following the procedure described in Sect. 3, by also applying the incompleteness correction and the statistical field decontamination. The results (star counts for the He-Clump and bright RGB and the corresponding bolometric luminosities) are reported in Table 4. In NGC 419 star counts and luminosities have been computed excluding the innermost region (with a radius of $20''$), where completeness at the He-Clump magnitude level drops down to 60% (as shown in Fig. 3).

Fig. 7 and 8 plot the resulting observables for the four SMC clusters (black points) presented in this study and for the LMC clusters (grey points) discussed in Paper I and II. Theoretical predictions for the $[M/H] = -0.33$ and -1.35 dex (solid and dashed line respectively) metallicities are also plotted for comparison.

The cluster NGC 419 displays population ratios (both in counts and luminosities) slightly higher with respect to the theoretical predictions (similarly to the LMC cluster NGC 1783 in Paper II) but still consistent with the occurrence of the RGB phase transition. NGC 339, 361 and 416 show N_{RGB}/N_{He-Cl} ratios somewhat in between the two model predictions. Their location is consistent with our photometric estimates of the cluster metallicity (see Table. 2), slightly higher than the ones obtained by Mighell, Sarajedini & French (1998).

8. Conclusions

By using high-quality near IR photometry of four SMC stellar clusters with intermediate ages we derived new photometric metallicities. All the observed clusters show similar metallicities ($[\text{Fe}/\text{H}] \sim -1$) with only a weak dependence with the age. Actually, the Age-Metallicity Relation for the SMC is not well known and the different metallicity indicators, namely stellar clusters, planetary nebulae, field stars, still exhibit strong discrepancies. The most recent survey of SMC field giants based on Ca II triplet by Carrera et al. (2008) indicates a value of $[\text{Fe}/\text{H}] \sim -1$ dex in the age range between ~ 3 and ~ 10 Gyr, and $[\text{Fe}/\text{H}] \sim -0.7$ dex at ~ 1 Gyr.

Furthermore, we investigated the contribution of the AGB and RGB evolutionary stages to the total cluster luminosity. The cluster NGC 419, with an age of ~ 1 Gyr, exhibits population ratios for AGB and RGB that follow the behaviour already observed in the LMC clusters for objects of similar age. The other 3 clusters, with older ages in the ~ 5 -7 Gyr range show a negligible ($\sim 6\%$) luminosity contribution by the AGB, lacking bright C-stars, and an increasing contribution by the RGB population with respect to clusters of younger ages like NGC 419 and those in the LMC. We find a general agreement between the empirical population ratios and those predicted by theoretical models at $[\text{M}/\text{H}] = -1.35$ dex.

We warmly thank the anonymous referee for his/her useful suggestions. This research was supported by the Ministero dell'Istruzione, dell'Università e della Ricerca and it is part of the Progetti Strategici 2006 granted by the University of Bologna

REFERENCES

- Bessell, M. S. & Brett, J. M., 1988, *PASP*, 100, 1134
- Carrera, R., Gallart, C., Aparicio, A., Costa, E., Mendez, R. A., & Noel, N. E. D., 2008, arXiv0806.4465
- Carretta, E., & Gratton, R. G., 1997, *A&A*, 121, 95
- Chiosi, E., Vallenari, A., Held, E. V., Rizzi, L., & Moretti, A., 2006, *A&A*, 452, 179
- Cioni, M.-R. L., van der Marel, R. P., Loup, C., & Habing, H. J., 2000, *A&A*, 359, 601
- Cioni, M.-R., L., & Habing, H. J., 2003, *A&A*, 402, 133
- Da Costa, G. S., & Hatziditriou, D., 1998, *AJ*, 115, 1934

- de Freitas Pacheco, J. A., Barbuy, B., & Idiart, T., 1998, *ApJ*, 332, 19
- Dolphin, A. E., Walker, A. R., Hodge, P. W., Mateo, M., Olszewski, E. W., Schommer, R. A., & Suntzeff, N. B., 2001, *ApJ*, 562, 303
- Elson, R. A., & Fall, S. M. 1985, *ApJ*, 299, 211
- Ferraro, F. R., Messineo, M., Fusi Pecci, F., de Palo, M. A., Straniero, O., Chieffi, A., & Limongi, M., 1999, *AJ*, 118, 1738
- Ferraro, F. R., Montegriffo, P., Origlia, L., & Fusi Pecci, F., 2000, *AJ*, 537, 312
- Ferraro, F. R., Origlia, L., Testa, V. & Maraston, C., 2004, *ApJ*, 608, 772
- Frogel J. A., Persson, S. E., Aaronson, M., & Matthews, K., 1978, *ApJ*, 220, 75
- Frogel, J. A., Mould, J. R. & Blanco, V. M., 1990, *ApJ*, 352, 96
- Girardi, L., Chiosi, C., Bertelli, G., & Bressan, A. 1995, *A&A*, 298, 87
- Glatt, K., Grebel, E. K., Sabbi, E., Gallagher III, J. S., Nota, A., Sirianni, M., Clementini, G., Tosi, M., Harbeck, D., Koch, A., Kayser, A., & Da Costa, G., 2008, [arXiv:0807.3744v1](https://arxiv.org/abs/0807.3744v1)
- Harris, J., & Zaritsky, D., 2004, *A&A*, 127, 1531
- Hill, V., 1997, *A&A*, 324, 435
- Hunter, D. A., Elmegreen, B. G., Dupuy, T. J., & Mortonson, M., 2003, *AJ*, 126, 1836
- Maraston, C., 1998, *MNRAS*, 300, 872
- Maraston, C., 2005, *MNRAS*, 362, 799
- Mateo, M., 1988, *ApJ*, 331, 261
- Mighell, K. J., Sarajedini, A., & French, R. S., 1998, *ApJ*, 116, 2395
- Montegriffo, P., Ferraro, F. R., Origlia, L. , & Fusi Pecci, F, 1998, *MNRAS*, 297, 872
- Mucciarelli, A., Origlia, L., Ferraro, F. R., Maraston, C., & Testa, V., 2006, *ApJ*, 646, 939
- Rafelski, M., & Zaritsky, D., 2005, *AJ*, 129, 2701
- Renzini, A., & Buzzoni, A. 1986, in *Spectral Evolution of Galaxies*, ed C. Chiosi & A. Renzini (Dordrecht Reidel)

- Rich, R. M., Shara, M., Fall, S. M., & Zurek, D., 2000, *AJ*, 119, 197
- Rieke, G. H., & Lebofsky, M. J. 1985, *ApJ*, 288, 618
- Searle, L., Wilkinson, A., & Bagnuolo, W. G. 1980, *ApJ*, 239, 803
- Stetson, P. B., 1987, *PASP*, 99, 191
- Valenti, E., Ferraro, F. R., & Origlia, L., 2004, *MNRAS*, 351, 1204
- van den Bergh, S., 1981, *A&AS*, 46, 79
- Zaritsky, D., & Harris, J., 2004, *A&A*, 604, 167
- Zinn, R., & West, M. J., 1984, *ApJS*, 55, 45

Table 1. Main parameters of the sample of observed SMC clusters

Cluster	α (J2000)	δ (J2000)	s	Age^s (Gyr)	Age^{TO} (Gyr)	[Fe/H]	E(B-V)
NGC 419	01:08:17.35	-72:53:04.30	38	1.0	$1.2 - 1.6^e$	-0.60^b	0.08^d
NGC 416	01:07:58.82	-72:21:18.96	46	4.0	$5.6^a; 6^e$	$-0.80^b; -1.44^a$	0.08^a
NGC 361	01:02:10.09	-71:36:18.73	48	5.6	6.8^a	-1.45^a	0.07^a
NGC 339	00:57:46.19	-74:28:17.58	49	6.6	$5.0^a; 6^e$	$-0.70^b; -1.12^c; -1.50^a$	0.03^a

Note. —

Units of right ascension are hours, minutes and seconds, and units of declination are degrees, arcminutes, and arcseconds. The s-parameter is from Elson & Fall (1985). Age_s and Age_{TO} indicate the ages inferred by the calibration of s-parameter by Girardi et al. (1995) and by direct TO measurements, respectively. The ages are from (a) Mighell, Sarajedini & French (1998) and (e) Glatt et al. (2008). The metallicities are from (a) Mighell, Sarajedini & French (1998), (b) de Freitas Pacheco, Barbuy & Idiart (1998), (c) Da Costa & Hatziditriou (1998). The reddening are from (a) Mighell, Sarajedini & French (1998) and (d) Hunter et al. (2003).

Table 2. Integrated K_s magnitude, colors, luminosities and corresponding metallicities of the target clusters

Cluster	K_s	(H- K_s)	(J- K_s)	L_{tot}^k ($10^4 L_{\odot}^{k_s}$)	L_{tot}^{bol} ($10^4 L_{\odot}^{bol}$)	[Fe/H]
NGC 419	7.49	0.31	1.09	92.05	23.22	-0.96
NGC 416	8.68	0.13	0.68	30.76	14.01	-0.99
NGC 361	8.94	0.11	0.78	24.21	9.73	-1.08
NGC 339	9.38	0.10	0.72	16.14	6.84	-1.18

Note. — The derived photometric metallicities are calibrated in the Carretta & Gratton (1997) metallicity scale.

Table 3. Star counts and luminosities for AGB and C stars

Cluster	N_{AGB}^{obs}	N_{AGB}^{field}	N_{Carb}	L_{AGB}^k/L_{tot}^k	N_{Carb}/L_{tot}^{bol}	N_{Carb}/L_{tot}^k	L_{Carb}^k/L_{tot}^k
NGC 419	21	0	12	0.54	0.53	0.13	0.38
NGC 416	1	0	0	0.04	0	0	0
NGC 361	1	0	0	0.06	0	0	0
NGC 339	1	0	0	0.08	0	0	0

Table 4. Star counts and luminosities for RGB and He-Clump stars

Cluster	N_{RGB}	$N_{He-Clump}$	L_{RGB}^{bol} ($10^4 L_{\odot}^{bol}$)	$L_{He-Clump}^{bol}$ ($10^4 L_{\odot}^{bol}$)
NGC 419	263	608	8.69	3.85
NGC 416	190	299	5.47	1.66
NGC 361	109	180	4.25	1.23
NGC 339	107	188	3.09	1.20

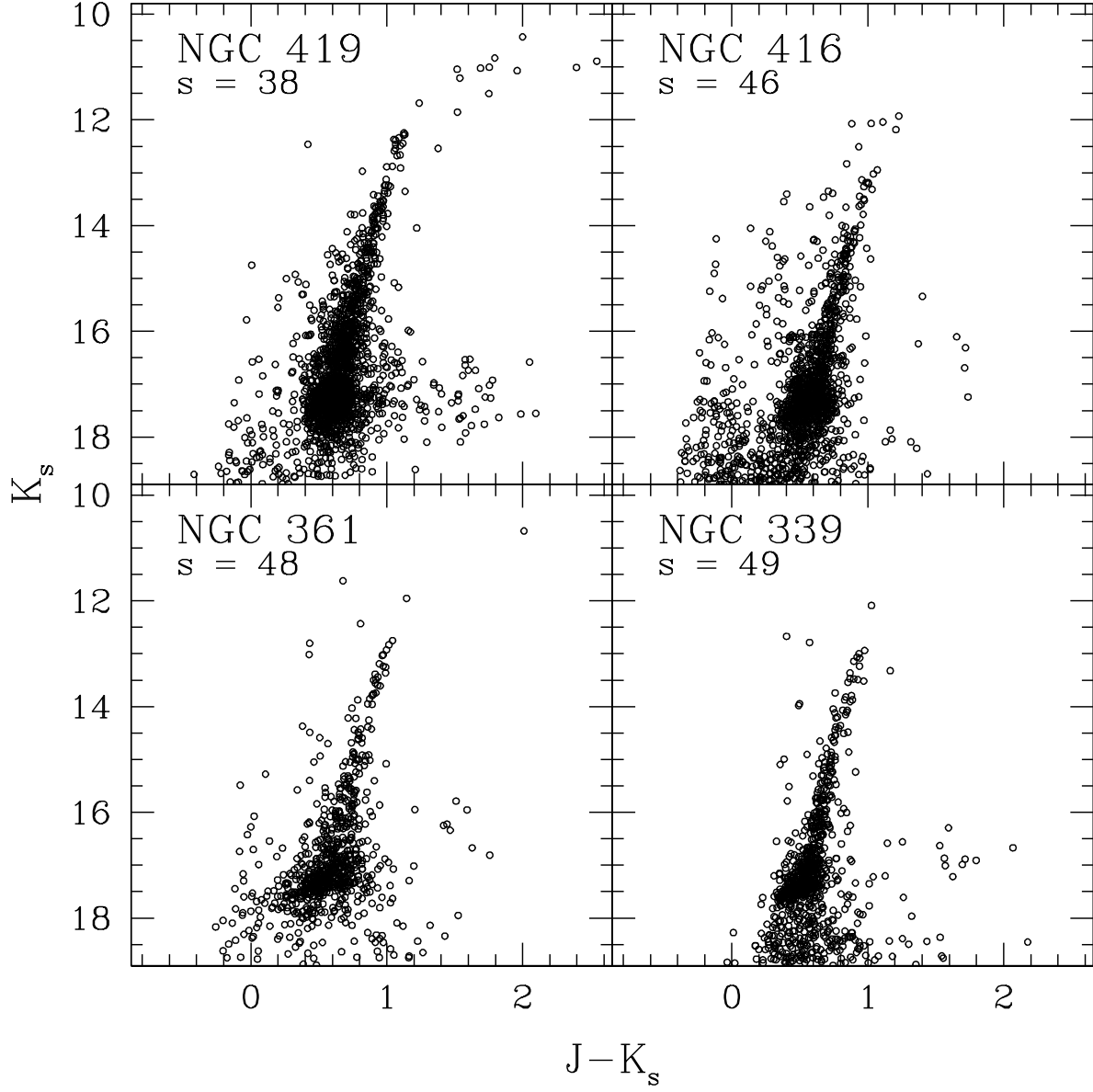


Fig. 1.— Observed $(K_s, J-K_s)$ CMDs of the four observed SMC clusters.

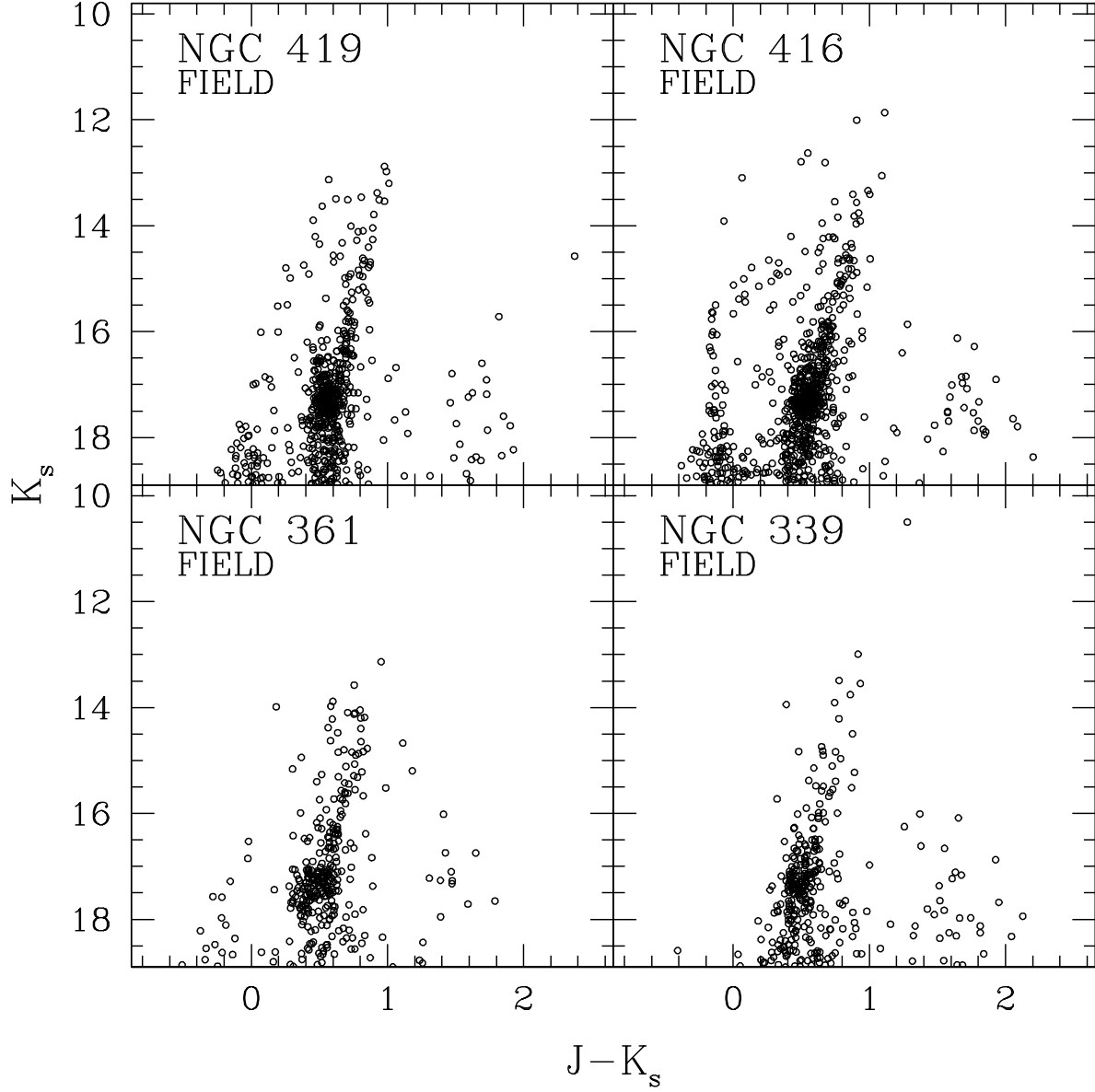


Fig. 2.— Observed $(K_s, J-K_s)$ CMDs of the fields adjacent to the four observed SMC clusters.

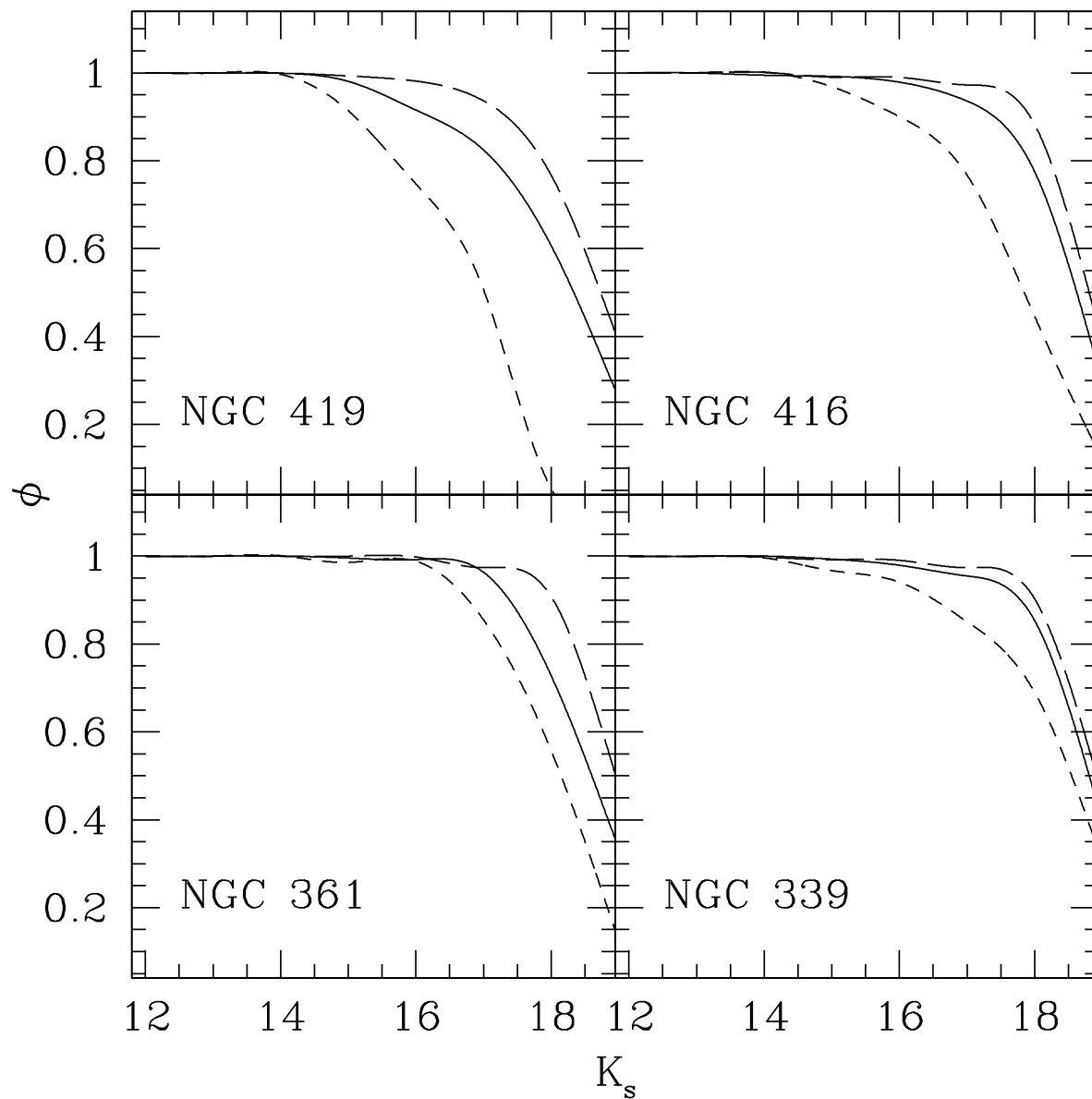


Fig. 3.— Completeness curves for the four SMC clusters. Short-dashed curves represent the inner region ($r < 20''$), solid lines the region between 20 and $\sim 60''$, and long-dashed lines the region between ~ 60 and $90''$.

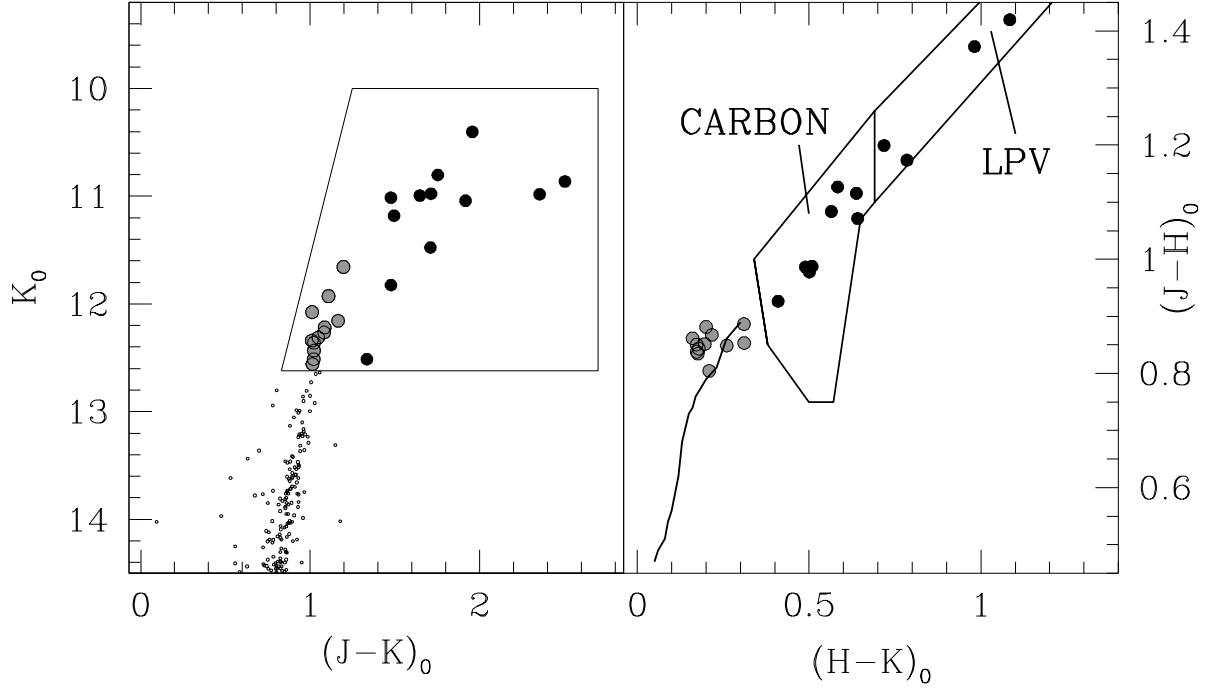


Fig. 4.— Cumulative, dereddened (K_0 , $(J-K)_0$) CMDs for the entire cluster sample, with overplotted the box used to select the AGB population. Grey points indicate the O-rich AGB stars and the black points the C-rich AGB stars.

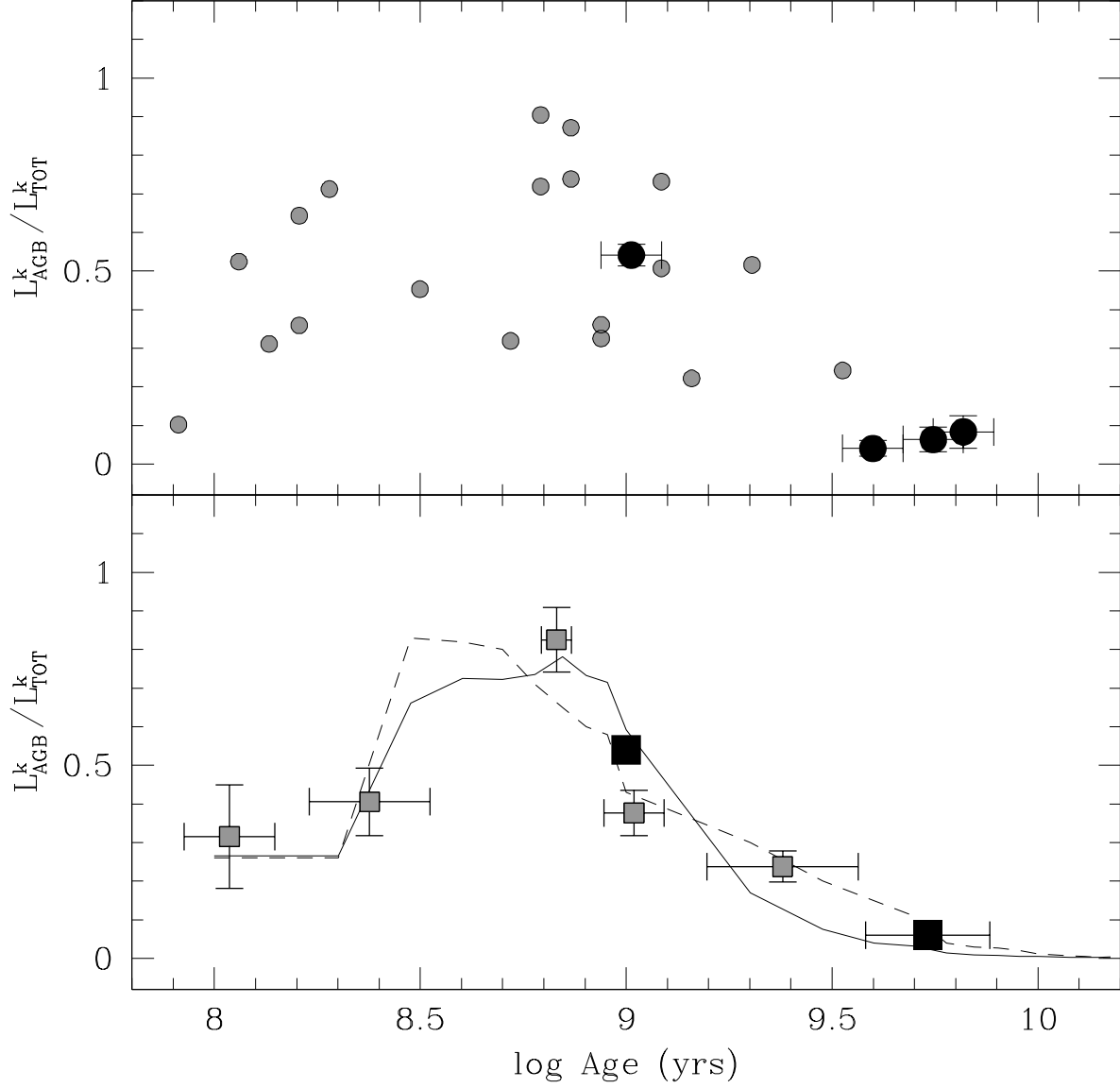


Fig. 5.— Top: Observed AGB contribution to the total cluster K_s -band luminosity as a function of the age. The black points indicate the SMC clusters. The grey points indicate the LMC clusters studied in Paper II. Bottom: Mean and standard deviation of the same ratio with the clusters grouped into age-bins. Theoretical predictions for the temporal evolution of the entire AGB (both Early and Thermal-Pulse AGB) at different metallicities are overplotted: solid line indicates the model computed at $[M/H] = -0.33$ and dashed line at $[M/H] = -1.35$.

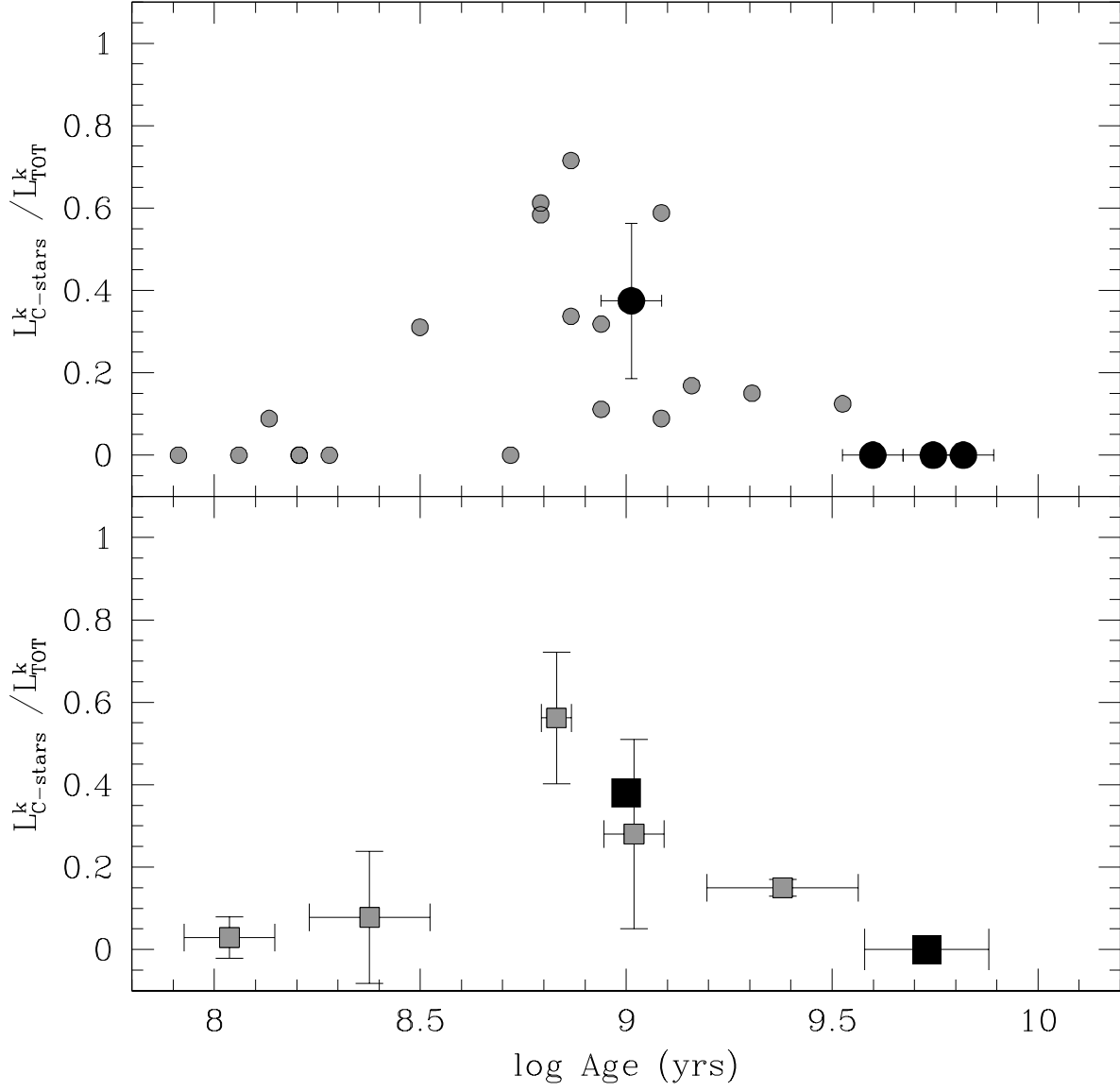


Fig. 6.— Top: Observed C-star contribution to the total cluster K_s -band luminosity as a function of the age. The black points indicate the SMC clusters. The grey points indicate the LMC clusters studied in Paper II. Bottom: Mean and standard deviation of the same ratio with the clusters grouped into age-bins.

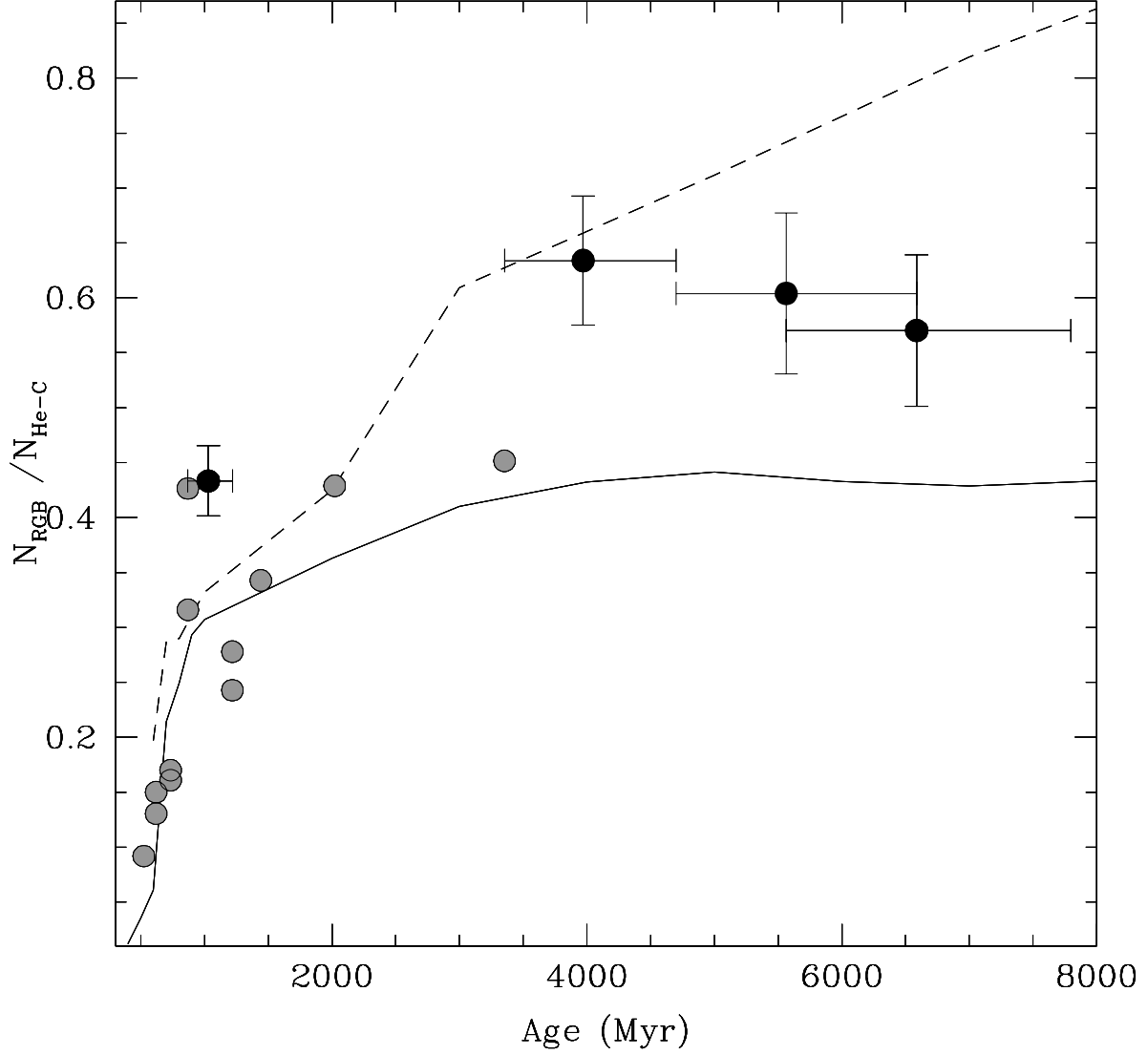


Fig. 7.— Behaviour of the number counts of RGB stars normalized to the He-clump stars as a function of the age. Same symbols of Fig. 5. Solid and dashed lines represent the theoretical predictions computed by using canonical models and global metallicity of $[M/H]=-0.33$ (solid line) and -1.35 (dashed line).

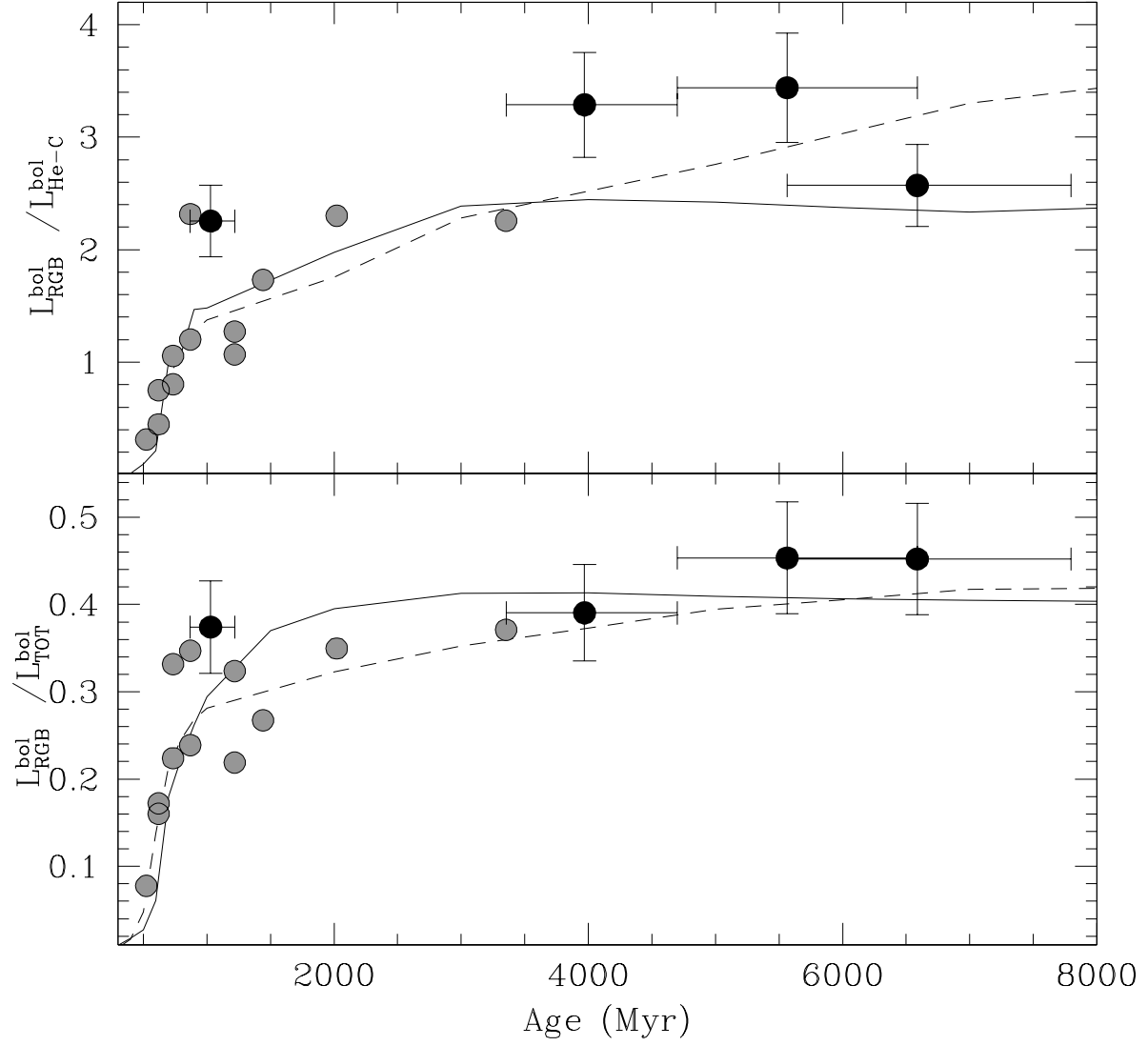


Fig. 8.— Top: Bolometric luminosity of the RGB normalized to the He-clump as a function of the age for the observed MC clusters. Same symbols of Fig. 5. Bottom: Bolometric luminosity of the RGB normalized to the total luminosity for the same clusters.